J. Synchrotron Rad. (1998). **5**, 268–274

High-Resolution High-Count-Rate X-ray Spectroscopy with State-of-the-Art Silicon Detectors

L. Strüder,[a]* C. Fiorini,[b] E. Gatti,[b] R. Hartmann,[a] P. Holl,[c] N. Krause,[a] P. Lechner,[c] A. Longoni,[b] G. Lutz,[b] J. Kemmer,[c] N. Meidinger,[a] M. Popp,[a] H. Soltau,[c] U. Weber[d] and C. von Zanthier[c]

[a]MPI für Extraterrestrische Physik, Halbleiterlabor, Paul-Gerhardt-Allee 42, D-81245 München, Germany, [b]Politecnico di Milano, Piazza Leonardo da Vinci 32, 20133 Milan, Italy, [c]KETEK GmbH, Am Isarbach 30, 85764 Oberschleissheim, Germany, and [d]MPI für Physik, Halbleiterlabor, Paul-Gerhardt-Allee 42, D-1245 München, Germany.
E-mail: lts@mpe-garching.mpg.de

(*Received 4 August 1997; accepted 20 October 1997*)

For the European X-ray multi-mirror (XMM) satellite mission and the German X-ray satellite ABRIXAS, fully depleted pn-CCDs have been fabricated, enabling high-speed low-noise position-resolving X-ray spectroscopy. The detector was designed and fabricated with a homogeneously sensitive area of 36 cm^2. At 150 K it has a noise of 4 e^- r.m.s., with a readout time of the total focal plane array of 4 ms. The maximum count rate for single-photon counting was 10^5 counts s^{-1} under flat-field conditions. In the integration mode more than 10^9 counts s^{-1} can be detected at 6 keV. Its position resolution is of the order of 100 μm. The quantum efficiency is higher than 90% from carbon *K* X-rays (277 eV) up to 10 keV. New cylindrical silicon drift detectors have been designed, fabricated and tested. They comprise an integrated on-chip amplifier system with continuous reset, on-chip voltage divider, electron accumulation layer stabilizer, large area, homogeneous radiation entrance window and a drain for surface-generated leakage current. At count rates as high as 2×10^6 counts cm^{-2} s^{-1}, they still show excellent spectroscopic behaviour at room-temperature operation in single-photon detection mode. The energy resolution at room temperature is 220 eV at 6 keV X-ray energy and 140 eV at 253 K, being achieved with Peltier coolers. These systems were operated at synchrotron light sources (ESRF, HASYLAB and NLS) as X-ray fluorescence spectrometers in scanning electron microscopes and as ultra low noise photodiodes. The operation of a multi-channel silicon drift detector system is already foreseen at synchrotron light sources for X-ray holography experiments. All systems are fabricated in planar technology having the detector and amplifiers monolithically integrated on high-resistivity silicon.

Keywords: silicon drift detectors; charged-coupled devices; high count rate; high-resolution X-ray spectroscopy.

1. Introduction

For several years, modern semiconductor detectors have been the prime choice for the measurement of nuclear radiation in various scientific fields. In satellite missions for astrophysics, silicon sensors are used as direct-imaging and/or spectroscopic detectors for near-IR, visible and X-ray photons (Bignami *et al.*, 1990). Equally, in other fields of research, *e.g.* at synchrotron sources and in material characterization systems, high 'event throughput' detectors are required. Large quantities of silicon detectors are operational in high-energy physics experiments as position-sensitive particle detectors.

In contrast, up to now, the industrial availability of semiconductor detectors for X-ray spectroscopy is mainly restricted by the relatively old concepts of Si(Li) and HPGe sensors.

This article will describe briefly the relevant concepts of modern high-resolution silicon detectors that have recently been developed, fabricated and tested for photons in the energy band 1–20 keV. These detectors make available a sensitive volume of the whole wafer thickness of about 300 μm. The more sophisticated concepts allow electronic noise levels close to 1 e^- r.m.s. due to their small readout capacitance and the integration of the first amplification stage onto the detector chip. Several prototype systems for industrial applications have already been manufactured and implemented in larger systems.

Two examples of detector systems already operational will be discussed: (i) the fully depleted X-ray pn-CCD for the X-ray multi-mirror (XMM) satellite mission of the European Space Agency (ESA) and for the German ABRIXAS satellite, both to be launched in 1999; (ii) the silicon drift detector for X-ray fluorescence analysis in scanning electron microscopes and, recently, in applications in EXAFS experiments and in X-ray holography. The conceptually more advanced depleted p-channel junction

field-effect transistor (DEPFET) and the depleted p-channel metal-oxide-semiconductor transistor (DEPMOS) systems will not be considered, because fully operational multi-pixel systems do not yet exist. All detector systems described below were designed, fabricated and tested in the MPI-Halbleiterlabor, Munich.

2. Basic concepts

In order to understand the basic functional principles of modern silicon radiation detectors, four aspects must be considered: (i) the charge generation in silicon, (ii) the reverse-biased diode as the basic radiation counter element, (iii) the sideward depletion of a semiconductor leading to the silicon drift chamber principle, and (iv) the amplification principles of on-chip electronics to obtain noise figures close to 1 e^- r.m.s.

2.1. *Charge generation*

The interaction of a photon or a charged particle with the detector bulk results in the generation of electron–hole pairs. The relation between the absorbed energy and the number of pairs is linear and independent of the kind of interaction and of the nature of the absorbed radiation. Only for the absorption of soft X-rays with energies less than 1000 eV is a non-linearity of some percent known (Lechner & Strüder, 1995).

2.2. *Reverse-biased diode*

In order to detect and analyse the radiation which is absorbed in the semiconductor material, it is necessary that the charge, which is generated by ionization, can be collected without loss. In normal semiconductor material the high number of electrons and holes, which are present due to the doping, make the measurement of an additional small number of charge carriers impossible. However, the depletion layers of rectifying contacts or pn-junctions are free of charge carriers and can be used for this purpose. By applying a reverse bias on the pn-junction, the width w of the depletion layer can be increased and the efficiency of the detector improves according to

$$w = \left\{[2\varepsilon_0\varepsilon_r(U - U_D)/q](N_A + N_D)/(N_A N_D)\right\}^{1/2}. \quad (1)$$

U is the bias voltage and U_D is the diffusion or built-in voltage, typically of the order of 0.5 V for a standard p^+n junction, ε_0 and ε_r are the dielectric constants, and N_A and N_D are the concentration of acceptors and donors. In this zone, w, free of mobile charge carriers having an electric field, linearly increasing with w the separation and drift of the electron–hole pairs, originating from converted X-rays, occurs. As can be seen from the above equation for the abrupt pn-junction, the extension of the depletion layer into the n- and p-area of the semiconductor is inversely proportional to the doping concentration, N_A and N_D, respectively. In practice, for semiconductor detectors, highly asymmetric pn-junctions with a very shallow p^+ doping on a very weakly doped n-substrate are used. Under these conditions (and $U \gg U_D$) the depletion layer expands only into the high-resistivity bulk material and the above equation simplifies to

$$w = (2\epsilon_0\epsilon_r U/qN_D)^{1/2}, \quad (2)$$

e.g. for a 9 kΩ cm n-type silicon wafer about 30 V reverse voltage is needed to completely deplete a 280 µm-thick wafer, resulting in a sensitive layer of the whole wafer thickness. If the Poisson equation, the basis of equation (1), is numerically solved in two dimensions, the electrical potential of a silicon drift chamber can be calculated as shown below.

2.3. *Silicon drift chamber principle*

In 1983 Gatti and Rehak proposed a new detector scheme based on sideward depletion (Gatti & Rehak, 1984). The idea is that a large semiconductor wafer of *e.g.* high-resistivity n-type silicon can be fully depleted from a small n^+ ohmic contact positively biased with respect to the p^+ contacts covering both surfaces of the silicon wafer.

In the standard configuration the depletion zones will expand from all rectifying junctions simultaneously as long as the ohmic access from the n^+ anode to the entire (non-depleted) bulk is not interrupted. At a given voltage the depletion zones propagating from the p^+ areas touch each other. Under this condition the former conducting electron channel, symmetrically located in the middle of the substrate between the p^+ implants, will abruptly disappear. At this moment the depletion of the whole wafer is completed at a voltage which is four times lower than the voltage needed to deplete a simple diode of the same thickness [see equation (2)]. Under the above-described condition the electron potential energy in a section perpendicular to the wafer surface has a parabolic shape, with an electron potential minimum in the middle of the wafer.

The silicon drift chamber is derived from the principle of sideward depletion by adding an electrical field, which forces the electrons to the n^+ readout anode. This is simply achieved by implantation of a parallel p^+ strip pattern at both sides of a semiconductor wafer and superimposing a voltage gradient at both strip systems. The direction of the voltage gradient is such that the n^+ readout anode has the highest positive potential, therefore collecting all the signal electrons accumulated in the potential minimum.

To simplify the fabrication technology, the strip system is replaced by a large area pn-junction at one side, which is used as a very homogeneous thin entrance window for the radiation (Kemmer *et al.*, 1987; Lechner *et al.*, 1996). A further improvement of this type of drift chamber uses cylindrical drift electrodes which force the signal electrons to a very small anode in the centre of the device from where they are transferred to the gate of an integrated JFET (see Fig. 1).

The electrical potential of the cylindrical silicon drift chamber is shown in Fig. 2 in a two-dimensional section perpendicular to the surface through the silicon wafer. It shows the potential energy for electrons of the device under test of Fig. 1 including all field strips and the central electron-collecting anode. The equipotential of the homogeneously doped radiation entrance window can be seen on the back, the field strips with their decreasing (negative) potential on the front side. There is no field-free region in the device and all electrons in the sensitive area are guided within less than 100 ns towards the readout node.

Recently, a novel drift detector concept, the controlled drift detector (CDD), was presented (Castoldi *et al.* 1997), adding to the excellent spectroscopic performance position-resolution for X-rays.

2.4. *On-chip amplification*

The traditional 'external' front-end and shaping amplifier concepts as used in conventional Si(Li) and HPGe systems will not be considered. We restrict ourselves to the amplification strategies that realise the first change of impedance or amplification directly on the detector chip. The advantages are: (i) by eliminating bond wires and pads the capacitance of the system can be heavily reduced, resulting in a lower equivalent noise level and less pick-up, (ii) problems of microphony are avoided, and (iii) more freedom in design is provided.

In our laboratory, three concepts for on-chip amplification have been developed: (*a*) the n-channel single-sided junction field-effect transistor (SSJFET) (Pinotti *et al.*, 1993), (*b*) the depleted PMOS or depleted p-type JFET detector–amplifier structures (DEPMOS or DEPFET) (Kemmer *et al.*, 1990), and (*c*) p-channel JFETs (Sampietro, Fasoli *et al.*, 1995). We have designed, fabricated and tested on-chip amplifiers of type (*a*) with an equivalent noise charge (ENC) of 2 e^- r.m.s., at 150 K. We achieved the low noise level by avoiding all kinds of stray capacitances between the readout node and ground. Using the silicon drift chamber principle, which guarantees a low detector capacitance, and the small on-chip FETs in the amplification stage, the total capacitive load, $C_{\rm tot}$, of the detector–amplifier is as small as 100 fF. With

$$Q = C_{\rm tot} U_{\rm in}$$

we can easily see that a small capacitance results in a significant change of voltage of the collecting anode. Q is the total charge arriving at the readout capacitance and $U_{\rm in}$ is the voltage change upon arrival of the signal charges at the (total) input capacitance $C_{\rm tot}$. A single electron arriving at the readout node would generate a voltage step of 1.6 μV, an already measurable quantity. State-of-the-art read nodes succeed in reducing the total capacitance to 20 fF. The limits of further progress in noise reduction are mainly given by the fabrication process technology and material properties.

With the help of Fig. 3 the basics of the amplification process of a SSJFET can easily be understood. Let us assume that the electrons, generated by the ionizing radiation, drift towards the readout anode. The voltage generated at the readout node is directly coupled to the p^+ gate of the n-channel transistor (source and drain are n^+ implants, the transistor channel is a deep n implant). The negative voltage on the p^+ gate reversely biases the junction, thus depleting the transistor channel, resulting in a current drop through the transistor. This change of current can be precisely detected.

3. Silicon detector systems

Two detector configurations will be presented: (i) the fully depleted X-ray pn-CCD as built for the XMM satellite mission, and (ii) the silicon drift chamber as built for spectroscopic investigations with synchrotron light, for fluorescent analysis, for particle counting and the parametrization of mixed radiation fields.

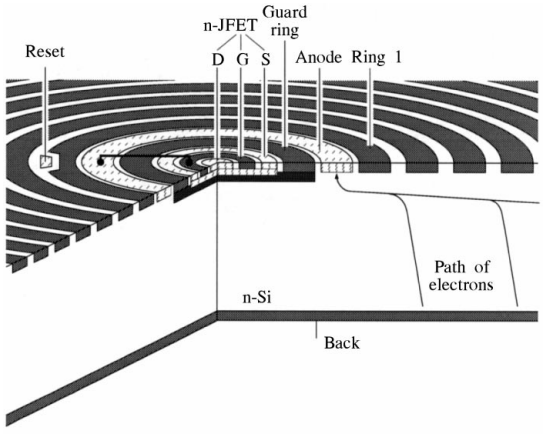

Figure 1
Central area of a cylindrical silicon drift chamber with an integrated amplifier for spectroscopic applications. The entire silicon wafer is sensitive to radiation.

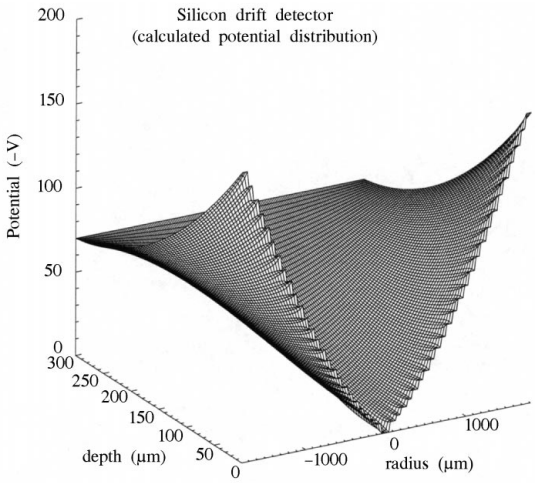

Figure 2
Potential energy distribution in a silicon drift chamber. The simulation applies to the whole detector shown in Fig. 1, including the electron-collecting readout node.

3.1. *Fully depleted charge-coupled devices (pn-CCDs)*

For ESA's XMM mission, to be launched in 1999, we have developed a 6 × 6 cm large monolithic X-ray CCD (Strüder *et al.*, 1990) with high detection efficiency up to 15 keV, low noise level (ENC $\simeq$ 5 e^-) and an ultrafast readout time of 4 ms. A schematic cross section, already showing some of the advantages of the concept, is displayed in Fig. 4. The concept allows for an optimum adaption of the pixel size to the X-ray optics, varying from 30 μm up to 300 μm pixel size. The energy response is higher than 90% at 10 keV because of the sensitive thickness of 300 μm. The low energy response is given by the very shallow implant of the p^+ back contact; the effective 'dead' layer is smaller than 150 Å (Hartmann *et al.*, 1996). The good time resolution is given by the parallel readout. A high radiation hardness is built in by avoiding MOS structures and by the fast transfer of the charge in a depth of more than 10 μm. The spatially uniform detector quality over the entire field of view is realised by the monolithic fabrication of 12 individually operated 3 × 1 cm large pn-CCDs on a single wafer. As the telescope system resolution on XMM is of the order of 15 arcsec with a focal length of about 7.5 m, the extension of a point source in the X-ray sky is about 500 μm in the focal plane. That is why a pixel size of 150 × 150 μm for the CCDs was chosen.

The best value for the readout noise of the on-chip electronics is 3 e^- r.m.s. at 150 K; typical values scatter around 5 e^- r.m.s. The charge transfer properties are as good as in standard CCDs, of the order of 1% charge loss from the last to the first pixel over a distance of 3 cm charge transfer. Fig. 5(*a*) shows a ^{55}Fe spectrum of a pn-CCD in a flat-field measurement resulting in a typical energy resolution of 130 to 140 eV (FWHM) (Soltau *et al.*, 1996). The low energy response of the system is shown in Fig. 6. The impact of the material properties of silicon and related impurities and their consequences for the operation of scientific-grade X-ray pn-CCDs, including the effects of radiation damage, is treated in detail by Meidinger *et al.* (1995).

In a single-photon counting mode the quantum efficiency was measured with respect to a calibrated position-sensitive proportional counter. In addition, a DC photocurrent measurement at the BESSY synchrotron in Berlin with a calibrated monochromator and reference detector is

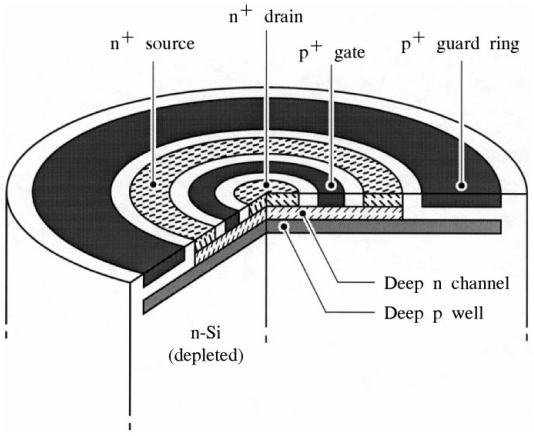

Figure 3
Schematic cross section through a single-sided junction field-effect transistor (SSFFET).

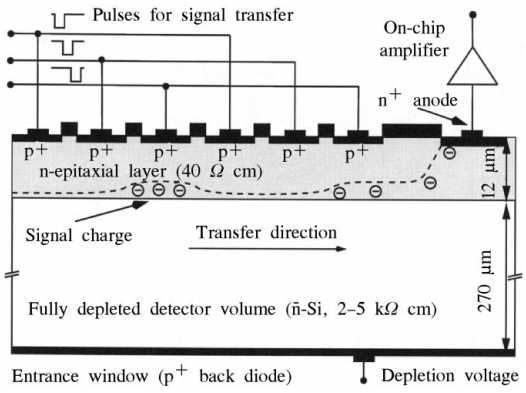

Figure 4
Schematic cross section of a fully sensitive pn-CCD. The radiation enters through the planar thin p^+ back diode. The sensitive thickness is 280 μm.

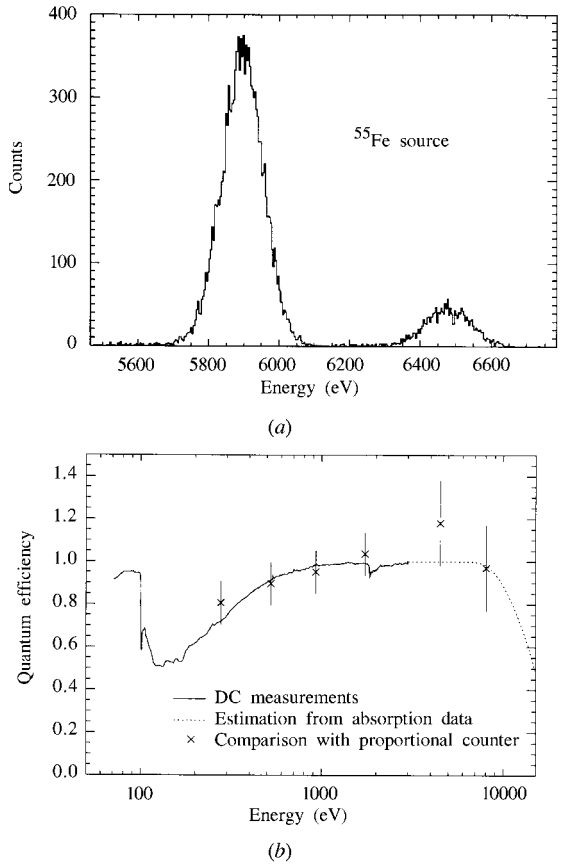

Figure 5
(*a*) ^{55}Fe spectrum with a pn-CCD in a flat-field measurement at a readout speed of 4 ms for a 3 × 1 cm large pn-CCD detector. The FWHM of the Mn $K\alpha$ peak is only 130 eV. (*b*) The measured quantum efficiency in a DC photocurrent measurement (solid line) and in a single-photon counting mode (×).

shown. Fig. 5(*b*) shows the single-photon counting data (×) and the DC photocurrent results in steps of 5 eV from 60 eV up to 3 keV. The single-photon data were taken with C *K*, O *K*, Cu *Lα*, Ti *Kα*, Cu *Kα* and Cu *Kβ* from an X-ray tube [see EOBB Final Report, ESA and Soltau *et al.* (1996)]. The quantum efficiency on the low-energy side was further improved with respect to the measurements in Fig. 5 shown above by increasing the drift field at the p^+ junction entrance window (Hartmann *et al.*, 1997). The readout electronics of the pn-CCD system are described by Strüder *et al.* (1990). A charge-sensing amplifier followed by a multicorrelated sampling stage, multiplexer and output amplifier (CAMEX64B JFET/CMOS chip) guide the pn-CCD pixel content as a voltage signal to a 10 MHz 12-bit flash ADC system. The whole system, *i.e.* CCD and CAMEX64B amplifier array, dissipates a power of 0.7 W, tolerable for the XMM satellite mission. A further increase of the readout speed can be made only at the expense of further increase of power, or a degradation of the noise performance.

We have tested the pn-CCD system in a single-photon counting mode in flat-field conditions at high count rates. If signal pile-up must be avoided, *i.e.* only one photon is allowed in one pixel, the maximum photon count rate is approximately 3000 counts $cm^{-2}\,s^{-1}$, leading to 10^5 counts s^{-1} for the full detector system. This was performed with a mechanical chopper wheel, preventing photons hitting the CCD during readout. The open position on the chopper wheel added another 6 ms of 'photon integration time' to the 4 ms readout time. Split events, *i.e.* events with electrons in more than one pixel, originating from a single photon, were reconstructed and summed to one photon event. In total, 75% of all events are single-pixel events, 23% are two-pixel events and 2% are events with three or four pixels involved. One single X-ray hit never affects more than four pixels.

If more than one photon is allowed to be in one single pixel, only the full well capacity of the CCD pixel limits the maximum detectable photon flux. About 1000 photons with an energy of 5 keV can be transferred per pixel, resulting in a count-rate limit more than 10^8 counts s^{-1} in the full detector. The charge-handling capacity of the individual pixels was tested with 5.486 MeV α-particles from a radioactive ^{241}Am source. More than 2×10^6 electrons can be properly transferred in every pixel.

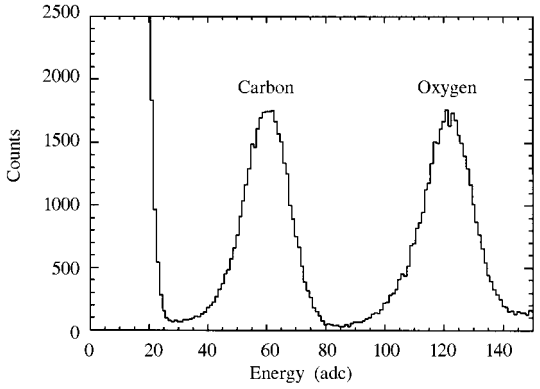

Figure 6
Spectrum of carbon *K* (277 eV) and oxygen *K* (525 eV) recorded with a pn-CCD.

3.2. *Silicon drift chambers for radiation monitoring and spectroscopy*

Silicon drift detectors (SDDs) already exist in a large variety of topologies and applications. We have designed, fabricated and tested the first SDDs with integrated readout electronics for X-ray spectroscopy (Hartmann *et al.*, 1994). They are cylindrical SDDs with a central anode, as shown in Fig. 1, with active areas, of 3.5 mm^2 and 5 mm^2.

The first experimental results of the devices show that at room temperature the intrinsic noise figures are of the order of 20 e^- translating in a width of the ^{55}Fe Mn *Kα* line of typically 220–230 eV at a shaping time of 500 ns for the 3.5 mm^2 and 5 mm^2 detectors. The bulk leakage current at 300 K contributing to the system noise is less than 1 nA cm^{-2}. At 263 K the equivalent noise charge is reduced to about 12 e^- r.m.s., *i.e.* slightly less than 160 eV FWHM at the Mn *Kα* line. Fig. 7 shows the system performance with a Peltier-cooled silicon drift detector at 253 K with a FWHM of 140 eV at 5.9 keV X-rays from the Mn *Kα* line from a ^{55}Fe source. At 220 K the noise decreases to 7.9 e^-, as shown experimentally, if an optimum digital shaping is used (Sampietro, Geraci *et al.*, 1995). The FWHM of an ^{55}Fe signal is then well below 140 eV, still being obtainable with thermoelectric cooling elements. All other relevant detector parameters are satisfactory: complete charge collection, spatially homogeneous response, reproducibility and long-term stability. Devices up to 1 cm^2 have been produced with one or more readout nodes. The largest device with 195 mm^2 area is realised having 39 readout nodes to achieve the high-

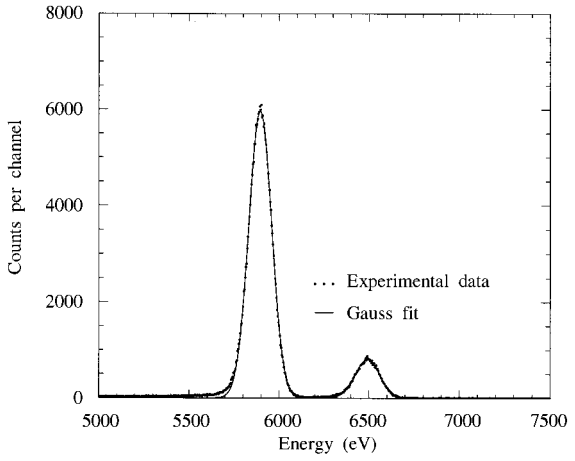

Figure 7
^{55}Fe spectrum recorded with a silicon drift chamber at 253 K (Peltier cooling) having a sensitive area of 5 mm^2 and a fully sensitive thickness of 280 μm. At a shaping time of 2 μs the equivalent noise charge (ENC) was 10.6 e^- r.m.s.. The FWHM at the Mn *Kα* line is 150 eV.

count-rate capability and the low noise level of the individual 5 mm^2 large subsystems (see Fig. 8). Multiplexing VLSI amplifiers are actually being developed to keep the complexity for the user at a reasonable level. We have tested the decrease of the spectroscopic performance as a function of X-ray count rate with the SDD at room temperature applying a signal-shaping constant of 250 ns (see Fig. 9). 10^5 counts s^{-1} can be detected at room temperature without a significant increase in the equivalent noise charge, *i.e.* without a broadening of the *e.g.* Mn $K\alpha$ line of the ^{55}Fe spectrum.

SDD devices have already been used as an X-ray fluorescence analysis detector in a scanning electron microscope (SEM) (RÖNTEC, 1997). A detector module, comprising a SDD cooled by a single-stage Peltier element, a ceramic substrate of 4 cm^2 with passive DC filters and on-chip thermometer, was successfully operated in an SEM field test. A six-anode detector (21 mm^2 of active area) has been operated in EXAFS measurements near room temperature at ESRF beamline No. 6 (Gauthier *et al.*, 1996). The good energy resolution at short shaping times (*e.g.* 162 eV FWHM with an ^{55}Fe source with a 250 ns shaping at 150 K) makes the detector very attractive for these experiments, typically carried out at synchrotron radiation facilities, where a high rate capability is needed, still with a simultaneous good energy resolution (Lechner *et al.*, 1996).

The compact design, the absence of liquid nitrogen for cooling, the high-count-rate capabilities, the non-sensitivity to microphonic noise pick-up and the lower price make these systems very attractive for commercial applications.

4. Count-rate considerations

In principle, a pixel detector, where every sensitive cell has its own amplifier and readout chain, would be the fastest device for high-resolution X-ray spectroscopy. But up to now no system is operational with properties which match the requirements for real experiments. The main limitations arise from the power consumption and, if the first amplification is not directly performed in the detector, from the noise performance of highly integrated analog external circuits.

The silicon drift detectors and fully depleted backside-illuminated pn-CCDs transfer the charges over larger distances to a readout node coupled to the gate of a junction field-effect transistor (JFET). While the pn-CCD guides the signal charges discreetly in time to the read node, this is performed continuously in a silicon drift detector. Therefore the position resolution in a cylindrical SDD with one readout node in the centre is as large as the area to which the drift fields expand (in our case about 2.5 mm), while in the CCD the spatial resolution is given by the pixel size. That is why the count-rate capabilities for single-photon counting are quite different.

4.1. *Count-rate capabilities of the pn-CCD system*

The pn-CCD system for the XMM satellite was not designed for high count rates but for high time resolution. Special operation modes were implemented (*e.g.* window modes, timing modes) to reduce the sensitive area to the benefit of a faster readout.

First we consider the full frame readout of the largest possible area (40 cm^2). In order to keep pile-up below 5%, we can process about 500 photons cm^{-2} $frame^{-1}$. If the full position resolution is required, a mechanical shutter can prevent radiation from hitting the detector during readout. In this case, 10 ms are needed to completely read out the system, *i.e.* at best, 5×10^4 events cm^{-2} s^{-1} can be detected in the single-photon counting mode. This finally leads to about 2×10^6 photons s^{-1} for the whole system maintaining full spatial resolution. Locally, but not for the whole system, the count rate per area can be increased by using the CCD as an analog storage in the so-called windowing and timing modes (Kendziorra *et al.*, 1997).

If no single-photon counting is required and the CCD is used as an imager instead of a photon counter, the count rate can be increased dramatically.

With a radioactive α-source the charge-handling capacity was tested up to 1.6×10^6 electrons per pixel. That means 1000 X-rays with an energy of 6 keV (each generating 1650 electron–hole pairs) can be collected in one

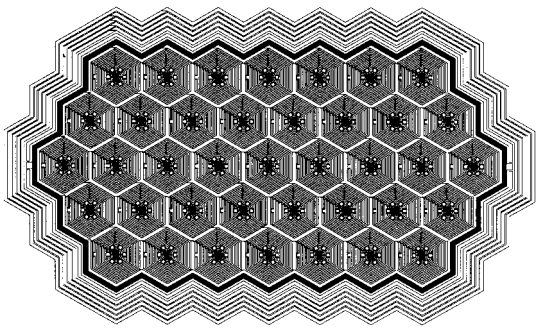

Figure 8
Layout of the 39-cell silicon drift detector array with 39 integrated on-chip amplifiers. The total active size of the system is 195 mm^2.

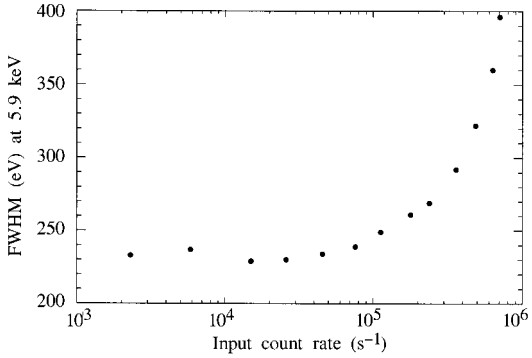

Figure 9
Measurement at room temperature of the count-rate-dependent energy resolution with an ^{55}Fe source. At 'low' count rates the FWHM is about 230 eV.

single pixel without any charge losses. If again the above-10 ms readout is applied, 100 frames can be recorded in one second, *i.e.* 10^5 photons pixel^{-1} s^{-1}. If we assume that only one-third of the potential capacity is filled with signal charges, still 5×10^9 photons s^{-1} can be recorded for the whole system. The full position resolution is still available but the very high count rate was (theoretically) obtained by performing integrated photon counting instead of spectroscopy.

4.2. *Count-rate capabilities of the silicon drift detector*

As shown in Fig. 9, each cell of the silicon drift detector can process approximately 10^5 events s^{-1}, if operated at room temperature. The increase of the FWHM at higher rates is mainly due to the processing electronics not yet due to the detector properties. The actual size of an SDD cell is 5 mm^2. This translates into a count rate of 2×10^6 cm^{-2} s^{-1} in single-photon counting spectroscopic mode.

For an experiment in X-ray holography, a 1000-cell detector will be built, equipped with low-noise front end JFET-CMOS VLSI electronics, comparable with the CAMEX64B amplifier being used with the pn-CCD. Such a system will have a total sensitive area of 50 cm^2 and a system count-rate capability of more than 10^8 counts s^{-1}.

5. Summary and conclusions

Silicon detectors are able to perform radiation monitoring and spectroscopy at moderate ambient conditions, low frequency acoustic noise and temperature. Because of the low capacitive readout anodes, noise levels below 5 e$^-$ r.m.s. at 150 K and around 10 e$^-$ r.m.s. at 300 K are obtainable. The detector leakage current adds to this intrinsic on-chip amplifier noise a temperature-dependent component, decreasing exponentially with decreasing temperature. Fully depleted pn-CCDs have shown an excellent performance for spatially resolved spectroscopy in a single-photon counting mode. A multi-purpose silicon drift detector (SDD) is operated for fast spectroscopic applications for synchrotron light users, for X-ray fluorescent applications, for dosimetry and as a low-noise photodiode for optical and calorimetrical applications.

The authors thank the staff of the MPI Halbleiterlabor and the Max Planck Institute für Physik und Extraterrestrische Physik for their continuous support. The perfect mounting and bonding of the devices by P. Solc and A. Kaltenberger is acknowledged. This research is supported by the German Space Agency DARA, the European Space Agency and the HCM program of the European Community.

References

Bignami, G. F., Villa, G. E., Boella, G., Bonelli, G., Caraveo, P., Chiappetti, L., Quadrini, M. E., Di Cocco, G., Trifoglio, M., Ubertini, P., Peres, G., Sciortino, S., Serio, S., Vaiana, G., Rothenflug, R., Vigroux, L., Koch, L., Rio, Y., Pigot, C., Cretolle, J., Gabreil, A., Foing, B., Atteia, J. L., Roques, J. P., Bräuninger, H., Pietsch, W., Predehl, P., Reppin, C., Strüder, L., Trümper, J., Lutz, G., Kendziorra, E., Staubert, R., Holland, A. D., Cole, R. E., Wells, A., Pounds, K., Lumb, D. A., Pye, J., Turner, M. J. L., Goodall, C. V., Ponman, T. J., Skinner, G. K. & Willmore, A. P. (1990). *SPIE*, **1344**, 144–153.

Castoldi, A., Guazzoni, C., Longoni, A., Gatti, E., Rehak, P. & Strüder, L. (1997). *IEEE*, **44**(5), 1724–1732.

Gatti, E. & Rehak, P. (1984). *Nucl. Instrum. Methods*, A**225**, 608–621.

Gauthier, Ch., Goulon, J., Moguiline, E., Rogalev, A., Lechner, P., Strüder, L., Fiorini, C., Longoni, A., Sampietro, M., Walenta, A., Besch, H., Schenk, H., Pfitzner, R., Tafelmeier, U., Misiakos, K., Kavadias, S. & Loukas, D. (1996). *Nucl. Instrum. Methods*, A**382**, 524–532.

Hartmann, R., Hauff, D., Krisch, S., Lechner, P., Lutz, G., Richter, R. H., Seitz, H., Strüder, L., Bertuccio, G., Fasoli, L., Fiorini, C., Gatti, E., Longoni, A., Pinotti, E. & Sampietro, M. (1994). *IEDM Technical Digest*, pp. 535–539. Piscataway, NJ: IEEE.

Hartmann, R., Hauff, D., Lechner, P., Richter, R., Strüder, L., Kemmer, J., Krisch, S., Scholze, F. & Ulm, G. (1996). *Nucl. Instrum. Methods*, A**377**, 191–196.

Hartmann, R., Strüder, L., Kemmer, J., Lechner, P., Fries, O., Lorenz, E. & Mirzoyan, R. (1997). *Nucl. Instrum. Methods*, A**387**(1/2), 241.

Kemmer, J., Lutz, G., Belau, E., Prechtel, U. & Welser, W. (1987). *Nucl. Instrum. Methods*, A**253**, 378–381.

Kemmer, J., Lutz, G., Prechtel, U., Schuster, K., Sterzik, M., Strüder, L. & Ziemann, T. (1990). *Nucl. Instrum. Methods*, A**288**, 92–98.

Kendziorra, E., Bihler, E., Kretschmar, B., Kuster, M., Pflüger, B., Staubert, R., Bräuninger, H., Briel, U., Pfeffermann, E. & Strüder, L. (1997). *SPIE*, **3114**, 155–165.

Lechner, P., Eckbauer, S., Hartmann, R., Richter, R., Strüder, L., Krisch, S., Soltau, H., Hauff, D., Fiorini, C., Gatti, E., Longoni, A. & Sampietro, M. (1996). *Nucl. Instrum. Methods*, A**377**, 346–351.

Lechner, P. & Strüder, L. (1995). *Nucl. Instrum. Methods*, A**354**, 464–474.

Meidinger, N., Strüder, L., Soltau, H. & von Zanthier, C. (1995). *IEEE,* **42**(6), 2066–2073.

Pinotti, E., Bräuninger, H., Findeis, N., Gorke, H., Hauff, D., Holl, P., Kemmer, J., Lechner, P., Lutz, G., Kink, W., Meidinger, N., Metzner, G., Predehl, P., Reppin, C., Strüder, L., Trümper, J. & von Zanthier, C. (1993). *Nucl. Instrum. Methods*, A**326**, 85–91.

RÖNTEC (1997). *X-Flash Detector – Product Information 4*. GmbH, Rudower Chaussee 6, Geb. 19.1/2, D-12489 Berlin, Germany.

Sampietro, M., Fasoli, L., Rehak, P. & Strüder, L. (1995). *IEEE Trans. Electron Devices*, **16**(5), 142–147.

Sampietro, M., Geraci, A., Fazzi, A. & Lechner, P. (1995). *Rev. Sci. Instrum.* **66**(11), 5381.

Soltau, H., Holl, P., Krisch, S., von Zanthier, C., Hauff, D., Richter, R., Bräuninger, H., Hartmann, R., Hartner, G., Krause, N., Meidinger, N., Pfeffermann, E., Reppin, C., Schwaab, G., Strüder, L., Trümper, J., Kendziorra, E. & Krämer, J. (1996). *Nucl. Instrum. Methods*, A**377**, 340–345.

Strüder, L., Bräuninger, H., Meier, M., Predehl, P., Reppin, C., Sterzik, M., Trümper, J., Cattaneo, P., Hauff, D., Lutz, G., Schuster, K. F., Schwarz, A., Kendziorra, E., Staubert, A., Gatti, E., Longoni, A., Sampietro, M., Radeka, V., Rehak, P., Rescia, S., Manfredi, P. F., Buttler, W., Holl, P., Kemmer, J., Prechtel, U. & Ziemann, T. (1990). *Nucl. Instrum. Methods*, A**288**, 227–235.